Molecular Pharmacology Fast Forward. Published on January 6, 2015 as DOI: 10.1124/mol.114.095729
This article has not been copyedited and formatted. The final version may differ from this version.

Translational downregulation of HSP90 expression by iron chelators in neuroblastoma cells.

Viktoryia Sidarovich, Valentina Adami, Pamela Gatto, Valentina Greco, Toma Tebaldi, Gian Paolo Tonini, Alessandro Quattrone

Laboratory of Translational Genomics, Centre for Integrative Biology, University of Trento, via delle Regole 101, 38123 Trento, Italy (V.S., P.G., V.G., T.T., A.Q.)

High-Throughput Screening Core Facility, Centre for Integrative Biology, University of Trento, via delle Regole 101, 38123 Trento, Italy (V.A.)

Neuroblastoma Laboratory, Onco/Hematology Laboratory, SDB Department, University of Padua, Pediatric Research Institute, Padua, Italy (G.P.T.)

Molecular Pharmacology Fast Forward. Published on January 6, 2015 as DOI: 10.1124/mol.114.095729
This article has not been copyedited and formatted. The final version may differ from this version.

RUNNING TITLE: Iron chelators inhibit HSP90 translation in neuroblastoma

CORRESPONDENCE SHOULD BE ADDRESSED TO:

Viktoryia Sidarovich, Centre for Integrative Biology, University of Trento, via delle Regole 101, 38123 Trento, Italy. Phone: +39 0461 282744, fax: +39 0461 283937, e-mail: viktoryia.sidarovich@unitn.it

Alessandro Quattrone, Centre for Integrative Biology, University of Trento, via delle Regole 101, 38123 Trento, Italy. Phone: +39 0461 283096, fax: +39 0461 283937, e-mail: alessandro.quattrone@unitn.it

MANUSCRIPT STATISTICS:

Text pages: 44

Figures: 5

References: 48

Abstracts words: 218

Introduction words: 744

Discussion words: 1499

Abbreviations: 7-AAD, 7-aminoactinomycin D; 17-AAG, 17-(Allylamino)-17-demethoxygeldanamycin; 8HQ, 8-hydroxyquinoline; CI, combination index; CPX, ciclopirox olamine; DEGs, differentially expressed genes, DFO, deferoxamine mesylate salt; DOHH, deoxyhypusine hydroxylase; DTPA, diethylenetriaminepentaacetic acid; Fa, fraction affected; FDA, Food and Drugs Administration; HSP, heat-shock protein; HT, holo-transferrin; IG50, inhibition of growth of 50%; IPA, Ingenuity pathway; MNA, *MYCN*-amplified; NB, neuroblastoma.

Molecular Pharmacology Fast Forward. Published on January 6, 2015 as DOI: 10.1124/mol.114.095729
This article has not been copyedited and formatted. The final version may differ from this version.

ABSTRACT

Iron is an essential cellular nutrient, being a critical cofactor of several proteins involved in cell growth and replication. Compared to normal cells, neoplastic cells have been shown to require a greater amount of iron, thus laying the basis for a promising anti-cancer activity of iron chelators. In this work we evaluated the effects of molecules with iron chelation activity on neuroblastoma (NB) cell lines. Of the 17 iron chelators tested, six reduced cell viability of two NB cell lines with IG_{50} below 10 μM; four of the six molecules - ciclopirox olamine (CPX), piroctone, 8-hydroxyquinoline, deferasirox – were also shown to efficiently chelate intracellular iron within the minutes after addition. Effects on cell viability of one of the compounds, CPX, were indeed dependent on chelation of intracellular iron and mediated by both G_0/G_1 cell cycle block and induction of apoptosis. By combined transcriptome and translatome profiling we identified early translational downregulation of several members of the heat-shock protein (HSP) group as a specific effect of CPX treatment. We functionally confirmed iron-dependent depletion of HSP90 and its client proteins at pharmacologically achievable concentrations of CPX, and we extended this effect to piroctone, 8-hydroxyquinoline and deferasirox. Given the documented sensitivity of NB cells to HSP90 inhibition, we propose CPX and other iron chelators as investigational antitumor agents in NB therapy.

Molecular Pharmacology Fast Forward. Published on January 6, 2015 as DOI: 10.1124/mol.114.095729
This article has not been copyedited and formatted. The final version may differ from this version.

INTRODUCTION

Neuroblastoma (NB) is the most common extracranial solid childhood cancer, derived from undifferentiated neural crest cells (Brodeur, 2003). It is a complex and heterogeneous disease, whose outcome – from spontaneous regression to rapid progression – is determined by many clinical and biological features, such as age at diagnosis, disease stage, numerical and structural chromosomal alterations, etc (Cheung and Dyer, 2013). Recent advances in understanding these molecular, cellular and genetic features of NB allowed of refining the classification of patients into risk groups, followed by more accurate therapy stratification. From one side, this led to reduction of cytotoxic treatments and thus adverse treatment-related late effects in patients with more favorable outcomes. From the other side, however, treatment of patients who currently have a poor prognosis is still a challenge, emphasizing the need of alternative approaches and calling for a shift from broad-spectrum chemotherapy to personalized molecularly targeted treatments (Cole and Maris, 2012).

Currently, amplification of *MYCN* remains the best-characterized genetic marker correlated with high-risk disease and poor prognosis (Huang and Weiss, 2013). Despite deregulation of MYCN is a hallmark of high-risk NB, being a transcription factor this protein is of very difficult druggability. Alternative pharmacological approaches focuses on MYCN mRNA, with the aim of either suppressing its production (Thiele *et al.*, 1985) or favoring its degradation (Burkhart *et al.*, 2003). Recently, we conducted a screen of FDA-approved drugs on a high-risk *MYCN*-amplified (MNA) NB cell line targeting yet another level of MYCN regulation (Sidarovich *et al.*, 2014). Specifically, we were looking for compounds able to modulate MYCN protein levels via its 3'UTR-dependent post-transcriptional control mechanisms. Among the four molecules selected as truly dependent on MYCN 3'UTR, three (doxorubicin, daunorubicin and epirubicin) were anthracyclines, a class of drugs used

Molecular Pharmacology Fast Forward. Published on January 6, 2015 as DOI: 10.1124/mol.114.095729
This article has not been copyedited and formatted. The final version may differ from this version.

in the first line treatment of NBs. The fourth molecule was an off-patent synthetic antimicrobial agent, ciclopirox olamine (CPX). Though originally developed for the topical treatment of cutaneous fungal infections, CPX has recently been reported to display preclinical efficacy as an effective anti-tumor agent in the treatment of various cancers (Clement *et al.*, 2002; Eberhard *et al.*, 2009; Zhou *et al.*, 2010; Song *et al.*, 2011; Ma *et al.*, 2012; Sen *et al.*, 2013). Moreover, its efficacy in treatment of hematologic malignancies is currently evaluated in a Phase I clinical study (Weir *et al.*, 2011; Minden *et al.*, 2014).

Interestingly, both anthracyclines and CPX shared a unique feature – ability to chelate iron. This observation made us willing to investigate more generally the chelation of iron as a potential therapeutic strategy in the treatment of NB. In fact, iron chelators have received considerable attention as potential antitumor agents over the last decade, owing to the avidity of cancer cells for iron (Richardson *et al.*, 2009; Torti and Torti, 2013). Many proteins involved in intracellular iron regulation have been shown to contribute to the malignant phenotype, thus making cancer cells more susceptible to iron deprivation as compared to their normal counterparts. The effect of iron chelators on cellular iron metabolism is complex, since they act on multiple molecular targets. Iron chelators have been referred to as regulators of iron-regulatory proteins, inhibitors of iron-dependent enzymes, compounds facilitating the redox cycling of iron to generate cytotoxic reactive oxygen species within tumors (Richardson *et al.*, 2009; Torti and Torti, 2013). In addition, a clear link between iron and various signaling pathways has been established, even though the detailed mechanism of iron-dependency is to be clarified. Thus, it is not surprising there are continuing efforts to improve the potency and selectivity of iron chelators against cancer cells.

We initiated this study to evaluate if the compounds with the reported iron-chelating properties are effective against NB. Our results show that a subset of tested molecules

Molecular Pharmacology Fast Forward. Published on January 6, 2015 as DOI: 10.1124/mol.114.095729
This article has not been copyedited and formatted. The final version may differ from this version.

potently reduced viability of NB cells and at the same time efficiently chelated intracellular iron. We further focused on a single iron chelator, CPX, and were able to show that CPX-mediated effects on cell viability were indeed iron-dependent and resulted from both deregulated cell cycle progression and induction of apoptosis. mRNA profiling performed on CPX-treated cells revealed translational downregulation of heat shock protein (HSP) family genes. The main chaperone HSP90, a known tumor target, was confirmed to be reduced at the protein level by CPX, and the effect was extended to the subset of iron chelators effective on NB cells. We therefore found that in NB cells HSP90 is inhibited by iron chelators of different chemical structure, opening to further evaluation of these molecules or their derivatives as potential NB drugs.

Molecular Pharmacology Fast Forward. Published on January 6, 2015 as DOI: 10.1124/mol.114.095729
This article has not been copyedited and formatted. The final version may differ from this version.

MATERIALS AND METHODS

Chemicals

CPX, deferoxamine mesylate salt (DFO), piroctone olamine, 8-hydroxyquinoline (8HQ), deferiprone, D-(–)-tagatose (7), 2,2'-bipyridyl, omadine, 2,3-dihydroxybenzoic acid, diethylenetriaminepentaacetic acid (DTPA), o-phenantroline, 2-picolinic acid, L-mimosine, ferrichrome, dexrazoxane, ferrozine, holo-transferrin (HT), cycloheximide were purchased from Sigma-Aldrich. Deferasirox was obtained from Sequoia Research Products, 17-(Allylamino)-17-demethoxygeldanamycin (17-AAG) from Tocris Bioscience. Topotecan and cisplatin were purchased from Enzo Life Sciences, calcein AM fluorescent dye from BD Biosciences.

Cell lines

The NB cell lines CHP134, KELLY, LA-N-2, NB69, SK-N-AS, SK-N-BE(2) and SK-N-SH were purchased from the European Collection of Cell Cultures (ECACC); CHP-212, HeLa and HEK-293 cell lines were purchased from American Type Culture Collection (ATCC) and SiMa from Deutsche Sammlung von Mikroorganismen und Zellkulturen GmbH (DSMZ). The cell line MCF7 was received from Banca Biologica e Cell Factory. All cell lines were cultured in humidified 37°C, 5% CO_2 incubator in media prepared following the instructions of the suppliers.

Viability assays

The cell viability was measured either by the AlamarBlue viability assay (Life Technologies) and xCELLigence real-time cell-analysis (RT-CA) DP system (Roche). Cells were plated in transparent 96-well plates at the pre-defined concentrations. For each cell line a control plate for “time zero” measurement was included along with experimental

Molecular Pharmacology Fast Forward. Published on January 6, 2015 as DOI: 10.1124/mol.114.095729
This article has not been copyedited and formatted. The final version may differ from this version.

plates. The AlamarBlue assay was typically performed on the day of compound addition for control plates and in 24-48 hours of treatment for experimental plates. The AlamarBlue reagent was added in an amount equal to 10% of the cell culture volume, and the plates were returned to an incubator. 7 hours later fluorescence was detected with excitation wavelength of 570 nm and emission wavelength of 600 nm using the Tecan Infinite M200 instrument. The percentage of viable cells was calculated using the following equations: (Ti-Tz)/(C-Tz)×100 if Ti≥Tz and (Ti-Tz)/Tz×100 if Ti<Tz, where Tz (time zero) is a fluorescence measurement at the time of drug addition (performed in control plates), while control growth (C) and test growth (Ti) are fluorescence measurements in the presence of a vehicle and a compound of interest, respectively. To evaluate in real-time the effect of CPX on viability of CHP134 cells, 8000 cells were plated in 16-well E-plates and 24 hours later were treated with increasing concentrations of CPX±HT. Cell viability was estimated based on the cell index recorded on the RT-CA DP system every 15 minutes. The cell index is derived from fluctuations in electrical impedance reflecting interaction of cells with microelectrodes integrated on the bottom of each well of the E-plate.

Three-dimensional (3D) multicellular spheroid model

CHP134 cell were plated in a round bottom ultra-low attachment 96-well plate (Corning) at concentration of 1000 cells per well in 100 µl complete media. After centrifugation at 300 g for 8 minutes cells were placed into an incubator. After 3 days spheroids were imaged using the high-content imaging system Operetta (PerkinElmer) and then treated with 0-20 µM CPX±HT following addition of 100 µl fresh media to each well. Images were acquired at 48, 72 and 96 hours of treatment and analyzed using Harmony software (PerkinElmer) that quantitated spheroids' area and roundness. The high-content output value was expressed as area*roundness.

Molecular Pharmacology Fast Forward. Published on January 6, 2015 as DOI: 10.1124/mol.114.095729
This article has not been copyedited and formatted. The final version may differ from this version.

Analysis of cell cycle by flow cytometry

Cell cycle analysis was performed on CHP134 cells treated with various concentrations of CPX for 24 hours using the Click-iT EdU Flow Cytometry Assay kit according to the protocol of the supplier (Life Technologies). Briefly, before harvesting the samples were incubated with 15 μM Click-iT EdU for 50 minutes. The samples containing 1×10^6 cells were fixed in 70% ethanol at -20°C overnight. The samples were permeabilized using Click-iT saponin-based permeabilization and wash reagent followed by EdU labeling with AlexaFluor 488 azide. The DNA content was measured using the 7-aminoactinomycin D (7-AAD, Life Technologies) stain at 2 μg/ml concentration. Finally, the samples were analyzed by flow cytometry on the BD FACSCanto II instrument. EdU-Alexa Fluor 488 azide and DNA content were detected using 488-nm excitation with the bandpass filter 530/30 and the longpass filter 670, respectively.

High-content imaging apoptosis assay

CHP134 cells growing in 96-well plates (CellCarrier, PerkinElmer) were treated with CPX (0-20 μM) for 24 and 48 hours. Cells were fixed by adding to culture media an equal volume of 8% formaldehyde. Fixed cells were incubated with a blocking/permeabilization solution (3% BSA, 0.3% Triton X-100 in PBS). The samples were stained using anti-active caspase 3 (ab13847, Abcam) as the primary antibody and Alexa Fluor 488 F(ab')2 fragment of goat anti-rabbit IgG (A-11070, Molecular Probes) as the secondary antibody. Finally, nuclei were stained with Hoechst 3342 (Molecular Probes). Images were acquired using the Operetta high-content system with a 20xLWD objective (PerkinElmer). Analysis was performed using the Harmony software (PerkinElmer).

Molecular Pharmacology Fast Forward. Published on January 6, 2015 as DOI: 10.1124/mol.114.095729
This article has not been copyedited and formatted. The final version may differ from this version.

Calcein-AM assay

Intracellular iron measurements were performed as described elsewhere (Eberhard *et al.*, 2009). Briefly, the culture media of cells growing in 6-well plates was aspirated and substituted with a PBS supplemented with 20 mM HEPES, 1 mg/ml BSA and 250 nM calcein-AM, pH 7.3. After 5 minutes incubation at 37°C, the cells were detached, washed and resuspended in PBS supplemented with 20 mM HEPES and 1 mg/ml BSA. The cells loaded with calcein were treated with iron chelators for 10 minutes. Changes in intracellular calcein fluorescence were measured by flow cytometry (FACSCanto, BD). The increase in fluorescence upon addition of iron chelators was calculated as percentage of the difference between median fluorescence measured in treated and untreated samples.

Extraction of polysomal and total RNA

CHP134 cells growing in 10 cm dishes were treated with a vehicle or 5 μM CPX for 24 hours. Total RNA was extracted using the RNeasy Plus Mini kit (Qiagen) following the instructions of the supplier and eluted in 50 μl of RNase-free water. To extract polysomal RNA, the following procedure was applied. The dishes with CHP134 cells were supplemented with 100 μg/ml cycloheximide and then returned to an incubator for 4 minutes. After removal of growing media, the cell-culture dishes were placed on ice and rinsed with phosphate buffer saline supplemented with cycloheximide. TH cells were lysed directly in the dishes by adding an ice-cold lysis buffer [10 mM NaCl, 10 mM $MgCl_2$, 10 mM Tris–HCl, pH 7.5, 1 % Triton X-100, 1 % sodium deoxycholate, 100 μg/ml cycloheximide, 0.2 U/μl RNase inhibitor, 1 mM DTT]. The lysates were collected with a cell scraper, pipetted into a microcentrifuge tube and after 5 minutes incubation on ice centrifuged for 10 min at 12000 g at 4 °C. The supernatants were fractionated by ultracentrifugation (Sorvall rotor, 100 min at 180000 g) through a 15–50 % linear sucrose

Molecular Pharmacology Fast Forward. Published on January 6, 2015 as DOI: 10.1124/mol.114.095729
This article has not been copyedited and formatted. The final version may differ from this version.

gradient containing 30 mM Tris–HCl, pH 7.5, 100 mM NaCl, 10 mM $MgCl_2$. Polysomal fractions were collected monitoring the absorbance at 254 nm on the Density Gradient Fractionation System (Teledyne Isco). Polysomal RNA was isolated after proteinase K treatment, phenol–chloroform extraction and isopropanol precipitation and finally resuspended in 50 μl of RNase-free water. RNA quality was assessed using the Agilent 2100 Bioanalyzer platform.

mRNA profiling

All the RNA samples were submitted to microarray analysis using the Agilent-014850 Whole Human Genome Microarray 4x44K G4112F chip from Agilent Technologies. Three biological replicates were done for each condition (control and treated with CPX at 90 minutes for total and polysomal RNA) and twelve hybridization arrays were obtained. cRNA probe generation as along with array hybridization, washing and staining were carried out according to the standard One-Color Microarray-Based Gene Expression Analysis (Quick Amp Labeling) protocol. Hybridized microarray slides were scanned with an Agilent DNA Microarray Scanner G2505C at 5 μm resolution with the manufacturer's software (Agilent ScanControl 8.1.3).

The scanned TIFF images were analyzed numerically and the background corrected using the Agilent Feature Extraction Software version 10.7.7.1 according to the Agilent standard protocol GE1_107_Sep09. The output of Feature Extraction was analyzed with the R software environment for statistical computing (http://www.r-project.org/) and the Bioconductor library of biostatistical packages (http://www.bioconductor.org/). Low signal Agilent probes, distinguished by a repeated "absent" detection call across the majority of the arrays in every condition, were filtered out from the analysis. Signal intensities across arrays were normalized with the quantile normalization algorithm. DEGs were determined

Molecular Pharmacology Fast Forward. Published on January 6, 2015 as DOI: 10.1124/mol.114.095729
This article has not been copyedited and formatted. The final version may differ from this version.

with the tRanslatome Bioconductor package, adopting a threshold based on the statistical significance of the change measured with a moderated t-test (p-value < 0.01) implemented in the Limma Bioconductor package. Translational efficiencies were calculated as the ratio of polysomal RNA and total RNA signals. All microarray data are available through the Gene Expression Omnibus database (http://www.ncbi.nlm.nih.gov/geo/) using the accession number GSE60675.

Gene enrichment analysis

The DAVID resource was used for enrichment analysis of the transcriptome and the translatome DEGs lists, using annotations from Gene Ontology (http://www.thegeneontology.org webcite), KEGG (http://www.genome.jp/kegg/ webcite), PFAM (http://pfam.xfam.org/), INTERPRO (http://www.ebi.ac.uk/interpro/). The significance of over-representation was determined using a p-value threshold of 0.05.

The Ingenuity pathway (IPA) software (IngenuitySystems, http://www.ingenuity.com) was used to assess the involvement in known pathways and networks of transcriptome and translatome DEGs. IPA uses the Fisher exact test to determine the enrichment of genes in canonical pathways. IPA also generates gene networks by using experimentally validated direct interactions stored in the Ingenuity Knowledge Base. The networks generated by IPA have a maximum size of 140 genes, and they receive a score indicating the likelihood of the genes to be found together in the same network due to chance. IPA networks were generated separately from transcriptome and translatome DEGs. A score of 4 was used as a threshold for identifying significant gene networks, indicating that there was only a 1/10000 probability that the presence of genes in the same network was due to chance.

Molecular Pharmacology Fast Forward. Published on January 6, 2015 as DOI: 10.1124/mol.114.095729
This article has not been copyedited and formatted. The final version may differ from this version.

Real-time quantitative PCR

To produce cDNA, 1 μg of total or polysomal RNA was reverse-transcribed according to the the protocol of the iScript cDNA synthesis kit (BioRad). PCR reactions were performed in a 10 μl reaction volume containing 5 ng template cDNA, 1×Kapa Probe Fast qPCR Universal Master Mix (2×) and 1×TaqMan Gene Expression assay of interest (Life Technologies, Supplemental Table 1). All reactions were carried out in 96-well plates (Hard-Shell Low-Profile 96-Well Skirted PCR plates, Bio-Rad) on the CFX96 real-time PCR detection system (Bio-Rad), followed by a regression Cq value determination method. The cycling conditions comprised 3 min polymerase activation at 95°C and 40 cycles at 95°C for 3 sec, 60°C for 20 sec and 72°C for 1 sec. qPCR amplification efficiency was calculated for each gene using a relative standard curve derived from a cDNA mixture of samples (a five-fold dilution series with five measuring points). The relative mRNA expression level of each gene was determined in Excel as described elsewhere (Hellemans *et al.*, 2007). The geometric mean of three reference genes (*HPRT1*, *SDHA*, *TBP*) was used for normalization of expression level of target genes.

Western blotting

Total proteins were extracted from pelleted cells in RIPA buffer followed by three freezing/thawing cycles. Following quantification with the Bradford reagent (Sigma), 10 μg total proteins were loaded and electrophoresed using sodium dodecyl sulfate polyacrylamide gel electrophoresis (SDS-PAGE) and transferred to nitrocellulose membranes (BioRad). After the blocking step, membranes were incubated with a primary antibody at +4°C overnight. Primary antibodies used were against HSP90 (Abcam, ab59459), HSP72 (Abcam, ab47455), HSC70 (Abcam, ab19136), RAF1 (Abcam, ab124452), TrkA (Millipore, 06-574), GAPDH (SantaCruz, sc-32233), tubulin (SantaCruz,

Molecular Pharmacology Fast Forward. Published on January 6, 2015 as DOI: 10.1124/mol.114.095729
This article has not been copyedited and formatted. The final version may differ from this version.

sc-53140). The secondary antibodies used were goat anti-mouse, anti-rat and anti-rabbit IgG-HRP (SantaCruz). Blots were imaged with the ChemiDoc XRS+ imaging system (BioRad) after addition of the ECL Prime detection reagent (Amersham).

Molecular Pharmacology Fast Forward. Published on January 6, 2015 as DOI: 10.1124/mol.114.095729
This article has not been copyedited and formatted. The final version may differ from this version.

RESULTS

Compounds with intracellular iron chelation properties decrease cell viability of NB cells

To assess the general anticancer activity of iron chelators in NB, we selected 17 commercially available compounds with known iron chelating properties (Supplemental Figure 1). The initial set of iron chelating compounds was tested for their effects on viability of CHP134 cells at two concentrations of 1 μM and 10 μM to cover a wider range of potential efficacy. After incubation for 48 hours cell viability was evaluated using the AlamarBlue assay. As shown in Figure 1A, this experiment identified 9 compounds that at 10 μM inhibited proliferation of CHP134 cells by at least 90% as compared to vehicle-treated control. The efficacy of 7 out of 9 compounds in reducing cell viability was confirmed in dose-response studies extended to two NB cell lines, CHP134 and SiMa (Figure 1B). Piroctone, CPX, 8-hydroxyquinoline (8HQ), and omadine resulted in lower IG50 values, while deferiprone, deferasirox and DFO were less effective. We then measured the ability of the selected compounds to bind intracellular iron in the calcein-AM assay (Breuer *et al.*, 1995b) to verify if this feature could be correlated with the suppression of cell viability. Calcein-AM, the acetoxymethyl ester of calcein, is a non-fluorescent cell permeant compound hydrolyzed by intracellular esterases into the impermeable fluorescent anion calcein. Calcein chelates intracellular iron and upon this its fluorescence is quenched; thus compounds able to displace intracellular iron from its complex with calcein result in increased fluorescence signal. The ability of the compounds to chelate intracellular iron was assessed by flow cytometry after 10 minutes of treatment at the final concentration of 10 μM with the exception of the poorly permeating chelator DFO, which was tested at 100 μM as the negative control. As shown in Figure 1C, piroctone, 8HQ, CPX and deferasirox

Molecular Pharmacology Fast Forward. Published on January 6, 2015 as DOI: 10.1124/mol.114.095729
This article has not been copyedited and formatted. The final version may differ from this version.

demonstrated the highest chelation ability, whereas deferiprone increased intracellular calcein fluorescence to a lesser extent. In contrast, DFO had no effect on calcein fluorescence even at 10 times higher concentration, which is in agreement with the fact that it penetrates the membrane and binds intracellular iron only after prolonged incubations (Breuer *et al.*, 1995a).

Of note, the extent of anti-proliferative effects of individual iron chelators not always could be linked purely to their capacity to chelate iron (compare Figure 1B and C). Indeed, the efficiency of iron chelators acting via iron sequestration mechanisms is determined by multiple factors. It depends on membrane permeability of the compounds, different iron complex formation constants and thus different capacity to sequester intracellular iron, presence of other metal ions competing with iron, capacity to access the active-site metal atom of cellular target enzymes (Clement *et al.*, 2002). For example, two iron chelators, DFO and deferiprone, have comparable iron complex formation constants (Clement *et al.*, 2002). However, deferiprone, a lipophilic compound that penetrates cellular membranes well, was able to sequester intracellular iron much more effectively than DFO (Figure 1C), which is hydrophilic and hence poorly permeable (Kalinowski and Richardson, 2005). Still, DFO inhibited viability of NB cells more efficiently than deferiprone (Figure 1B), indicating that the compounds affect distinct iron-dependent proteins/pathways with different efficiency. In fact, DFO was reported to inhibit deoxyhypusine hydroxylase (DOHH), an essential enzyme for maturation of the translation factor eIF5A, and DNA synthesis about 10 times more efficiently than deferiprone (Clement *et al.*, 2002).

A peculiar behavior observed in the calcein-AM assay for omadine resembled the decrease in fluorescence detected in cells loaded with excess of iron (data not shown), and thus could be interpreted as an increase of the intracellular iron pool. This observation, together with the high sensitivity of both CHP134 and SiMa cells to omadine, suggests a mechanism of

Molecular Pharmacology Fast Forward. Published on January 6, 2015 as DOI: 10.1124/mol.114.095729
This article has not been copyedited and formatted. The final version may differ from this version.

action not related to its property of binding intracellular iron. Indeed, the cytotoxic effects of omadine is almost immediate, not reversed upon withdrawal of the compound from the culture media or addition of iron, confirming a mechanism unrelated to iron binding (Kontoghiorghes *et al.*, 1986; Blatt *et al.*, 1989).

Taken together, three compounds - piroctone, CPX, and 8HQ - demonstrated prominent effect on NB cells viability that could be correlated to their marked avidity for intracellular iron. Two of them, piroctone and CPX, belong to the same class of hydroxypyridones, sharing very similar chemical structures. Of note, CPX is currently evaluated in a phase I clinical trial study in patients with relapsed and refractory hematologic malignancy (Minden *et al.*, 2014). Thus, CPX could potentially be rapidly repositioned as a new investigational antitumor agent in treatment of NB. CPX was therefore evaluated in secondary assays.

CPX is cytotoxic to neuroblastoma cells in an iron dependent manner

To further unveil the mechanism by which CPX inhibits cell viability, the studies were extended in a panel of cell lines, including MNA and non-MNA NB as well as non-NB cell lines (Figure 2A-C). CPX inhibited cell viability with an IG_{50} value in the range of 1-10 μM in eight out of nine NB cell lines, suggesting that this effect is not dependent on a specific NB cell-type. In a previous publication we demonstrated that CPX results in upregulation of MYCN protein within the first hours of treatment without a concomitant increase in MYCN mRNA levels (Sidarovich *et al.*, 2014). Therefore, a question arose if CPX-mediated effects on cell viability could be linked to MYCN levels in tested NB cell lines. Correlation analysis did not reveal any significant association between CPX IG_{50} values and MYCN copy number, mRNA expression and protein levels (Supplemental Figure 2). The effect of CPX on viability of non-NB cell lines was less marked: in MCF7

Molecular Pharmacology Fast Forward. Published on January 6, 2015 as DOI: 10.1124/mol.114.095729
This article has not been copyedited and formatted. The final version may differ from this version.

and HEK-293 cells IG_{50} values were around 10 μM, while HeLa cells did not reach the threshold of 50% inhibition at any concentration of CPX tested.

Next, we evaluated if the anti-proliferative activity of CPX on NB cells could be reversed either by removal of the compound from the culture media or by its supplementation with iron. First, CHP134 and SiMa cells were cultured in CPX-containing media for 6, 12, 24, 30, 36 and 48 hours and then in CPX-free media for up to 48 hours, when the number of viable cells was counted. As can be appreciated from Supplemental Figure 3, 6 hours of treatment did not affect cell viability at any concentration, indicating that there is a minimum time of cells' exposure to CPX treatment. Instead, the effects of 20 μM CPX exerted within the first 12 hours were not recovered in the subsequent 36 hours. Similarly, the impact of 6.6 μM CPX treatment for 24 hours was stable for the next 24 hours. These data indicate that CPX effects are persistent *in vitro* in a time- and concentration-dependent manner.

To determine if supplementation of media with iron was able to prevent CPX-induced cytotoxicity, we first evaluated in calcein-AM assay whether CPX was able to bind intracellular iron in selected NB cellular models, and then if the phenotype could be rescued by adding excess of iron. Indeed, 10 μM CPX significantly increased intracellular calcein fluorescence in 8 of 9 tested NB cell lines, whereas the potent extracellular chelator DFO had significantly lower effect on calcein fluorescence even at 10 times higher concentration (Supplemental Figure 4). Then, the tumor cells were treated with serial dilutions of CPX with and without iron supplementation to see if excess iron could abrogate CPX-induced toxicity. To increase iron levels specifically within the cells, iron was added in the form of holo-transferrin (HT), the diferric transferrin that releases iron intracellulary after it is bound to transferrin receptors and internalized into cells. The addition of excess iron delayed the cytotoxic effects of CPX in CHP134 cells (Figure 2A, D), indicating that

Molecular Pharmacology Fast Forward. Published on January 6, 2015 as DOI: 10.1124/mol.114.095729
This article has not been copyedited and formatted. The final version may differ from this version.

CPX-induced cytotoxicity was mostly dependent on iron chelation. However, the fact that CPX-mediated effects on viability of CHP134 and other NB cell lines were not completely abrogated by the addition of HT (Supplemental Figure 5) pointed out the presence of iron-independent mechanisms of CPX action (Sen *et al.*, 2013). Finally, the anti-proliferative effects of CPX on CHP134 cells grown as monolayers could be reproduced in a multicellular 3D spheroids model, and these effects could be, similarly to what happens in 2D cultures, partially prevented supplementing media with iron (Figure 2E and Supplemental Figure 6). These data indicate a potential therapeutic effect of CPX also *in vivo*.

CPX inhibits cell proliferation and induces apoptosis

We further evaluated whether CPX decreased cell viability through inhibition of proliferation and/or induction of cell apoptosis. Cell cycle distribution of CHP134 cells upon CPX treatment was assessed by flow cytometry using the Click-iT EdU chemistry multiplexed with 7-AAD DNA stain. At the two highest concentrations CPX effectively blocked CHP134 cells in the G_0/G_1 phase (Figure 3A and B). Treatment with 2 and 0.6 μM CPX resulted in a modest accumulation of the cells in S-phase and a contemporary decrease in the median fluorescent intensity of the EdU+ positive population (S-phase cells; Figure 3A−C). In other words, within the same period of time CPX-treated cells incorporated less EdU compared to control cells, which might be attributable to an inhibition of DNA synthesis. The effect seems to be concentration-dependent and not time-dependent, since similar cell cycle distribution was observed for 24 and 48 hours treatment with 2 or 0.6 μM CPX (Supplemental Figure 7). The data of cell cycle analysis were augmented by continuous long-term single-cell observations (Schroeder, 2011) demonstrating that upon treatment with higher concentrations of CPX cells do not undergo doubling and massive

Molecular Pharmacology Fast Forward. Published on January 6, 2015 as DOI: 10.1124/mol.114.095729
This article has not been copyedited and formatted. The final version may differ from this version.

cell death is observed, while the lower concentrations of CPX resulted in significantly prolonged doubling time (data not shown).

To evaluate the ability of CPX to cause apoptosis, a high-content imaging apoptosis assay was performed. As shown in Figure 3D, a strong increase in fluorescence intensity reflecting the activation of caspase-3 was observed upon CPX treatment in a concentration and time-dependent manner. The activation of caspase-3 was accompanied by the reduction in cell number. Concentration and time-dependent increase of caspase-3 activity upon the CPX treatment was confirmed using the Caspase-Glo 3/7 assay, in which the luminescence produced is proportional to the caspase-3/7 enzymatic activity (data not shown). Altogether, analysis of the data on cell cycle distribution and caspase-3 activation indicate that CPX-mediated inhibition of cell viability is associated with deregulated cell cycle progression and induction of apoptosis.

CPX induces translational downregulation of members of the heat shock proteins group

To enable a comprehensive overview of the gene expression response upon CPX treatment, a genome-wide multi-level transcriptome and translatome analysis was performed (Arava *et al.*, 2003; Tebaldi *et al.*, 2012). The polysomal mRNA (i.e. the mRNAs engaged in translation - the translatome) and the total mRNA (the total amount of transcribed mRNAs - the transcriptome) from CHP134 control cells and cells treated with 5 μM CPX for 90 minutes were extracted and quantified with gene expression microarrays. A total of 14196 genes resulted after data preprocessing, normalization and quality check with Bioconductor packages (see Materials and Methods). A scatter plot containing the whole set of transcriptome and translatome variations is displayed in Supplemental Figure 8A. The translatome response to CPX was poorly concordant with the transcriptome one, as

Molecular Pharmacology Fast Forward. Published on January 6, 2015 as DOI: 10.1124/mol.114.095729
This article has not been copyedited and formatted. The final version may differ from this version.

resumed by the low Spearman correlation value (0.33). This may be partially due to the short lapse of time at which cells were sampled. Differentially expressed genes (DEGs) as an effect of the CPX treatment were determined with the tRanslatome package (Tebaldi *et al.*, 2014) adopting a threshold based on the statistical significance of the change (the complete lists of DEGs are available in Supplemental Tables 2, 3, 4, 5). At this stage translational regulation, supposed to act with a faster dynamics than transcriptional regulation (Schwanhäusser *et al.*, 2011), encompasses the majority of observed changes, while transcriptional regulation requires more time to become effective and influence the cellular phenotype. Indeed, 1270 and 520 DEGs were registered in the translatome and transcriptome, respectively. Classes of DEGs are summarized in Figure 4A. Considering genes with significant variations only in one of the two levels, 68% of DEGs (in yellow and orange in Figure 4A) had significant changes only at the translatome level, 24% of DEGs (in blue in Figure 4A) changed significantly only at the transcriptome level. Comparing the two lists of genes, only 132 genes (8% of DEGs, in green in Figure 4A) showed significant homodirectional changes, reflecting the low concordance between transcriptional and translational movements. Therefore, the early response of CHP134 cells to CPX was mostly directed at the translational level, changing the loading on polysomes of several mRNAs. Finally, the microarray data were validated for 10 selected genes with disparate translational variations by qPCR, giving a high level of concordance (Supplemental Figure 8B).

In order to better understand the meaning of the cell response to the CPX treatment, we switched the focus of the analysis from movements of single genes to their clustered biological annotations. To this end, ontological enrichment analysis was performed on the lists of the transcriptome and translatome DEGs. Enrichments were calculated using annotations and statistical tests provided by the DAVID resource (Huang *et al.*, 2009) (see

Molecular Pharmacology Fast Forward. Published on January 6, 2015 as DOI: 10.1124/mol.114.095729
This article has not been copyedited and formatted. The final version may differ from this version.

Methods, the complete lists of significantly enriched terms are available in Supplemental Tables 6, 7, 8). From this analysis, heat shock proteins (HSPs) of the HSP70 family emerged as significantly and specifically enriched among translationally downregulated DEGs (Figure 4B, Supplemental Figure 8C and Supplemental Table 9 for the HGNC annotation of HSP protein families). An alternative approach, provided by the Ingenuity Pathway Analysis (IPA), was employed in order to detect the presence of interaction networks among the sets of differentially expressed genes. The whole set of IPA networks is available in Supplemental Table 10. This analysis confirmed the presence of a cluster of interconnected HSPs, including members of the HSP90 family, among translationally downregulated genes. All this evidence suggests that CPX treatment consistently reduces the translational efficiency (defined by the ratio of translatome and transcriptome signals) of HSP members. This phenomenon is displayed in Figure 4C, where the distributions of translational efficiency changes of HSP families are compared to the distribution of all microarray genes: HSP90 proteins show the most pronounced decrease in translation efficiency.

Iron chelators downregulate expression of the HSP90 protein.

Mammalian HSPs include several major families of molecular chaperones classified by their molecular weights: HSP90, HSP70, HSP60 and the small HSPs (Jego *et al.*, 2013). Family members of HSPs are expressed either constitutively or induced by many different stimuli. For example, the HSPA1A and HSPA8 transcripts, that were found to be translationally downregulated upon CPX treatment (Supplemental Figure 9), encode for two major cytoplasmic isoforms of the HSP70 protein: a ubiquitously expressed HSC70 and an inducible HSP72. Likewise, the most prominent members of the HSP90 family are the constitutively expressed HSP90 beta (encoded by *HSP90AB*) and the stress-inducible

Molecular Pharmacology Fast Forward. Published on January 6, 2015 as DOI: 10.1124/mol.114.095729
This article has not been copyedited and formatted. The final version may differ from this version.

HSP90 alpha (encoded by *HSP90AA*). In cancer cells, however, this differential expression pattern is commonly lost and increased constitutive expression of inducible isoforms is observed (Jego *et al.*, 2013).

In order to understand whether the effects of CPX on HSP group members evidenced by gene expression analysis as early as at 90 minutes of treatment are persistent in time, CHP134 cells were treated with 5 μM CPX for 24 hours followed by purification of total and polysomal mRNA and qPCR analysis. Downregulation of HSPs expression was detected also at 24 hours of treatment (Supplemental Figure 9). Though the degree of the polysomal mRNA downregulation of the measured HSPs remained approximately the same at 24 hours as compared to 90 minutes of treatment, upon prolonged treatment the transcriptome changes came up with the translatome level. At the same time transcriptional targets of hypoxia inducible factor-1 (HIF-1), which stability is increased upon iron depletion (Richardson *et al*., 2009), were upregulated at the transcriptome and translatome levels with high concordance (Supplemental Figure 10). This observation highlights that CPX effects on the group of HSPs follow a different pattern as compared to the well-documented HIF-1–mediated pathway.

HSP90 and HSP70 proteins play a crucial role in cancer cell survival. Together with additional proteins they form the chaperone machine used by cancer cells to ensure the correct conformation and stability of mutated and/or overexpressed oncogenic proteins, which otherwise would undergo degradation. Thus, cancer cells become often dependent on these HSPs, which are dispensable for the survival of normal cells (Trepel *et al.*, 2010; Jego *et al.*, 2013). Therefore, we focused our further attention on HSP90, HSC70 and HSP72, encoded by *HSP90AA*, *HSPA8* and *HSPA1A*, respectively. First, we tested if the expression variations observed for these genes at 24 hours are iron-dependent. To this purpose CHP134 cells were treated either with 5 μM CPX alone or with 5 μM CPX plus HT, or

Molecular Pharmacology Fast Forward. Published on January 6, 2015 as DOI: 10.1124/mol.114.095729
This article has not been copyedited and formatted. The final version may differ from this version.

with HT only. Subsequent qPCR analysis of total and polysomal mRNA revealed that CPX effectively reduced HSP90, HSP72 and HSC70 mRNA abundance in an iron-dependent manner (Figure 5A). Interestingly, CPX treatment resulted in marked fluctuations of the inducible HSP72 mRNA at the transcriptome level, while the changes at the level of translatome were somewhat buffered, again exemplifying the general ‘‘uncoupling’’ between transcriptome and translatome responses (Tebaldi *et al.*, 2012). At the protein level, CPX caused a robust reduction of HSP90 expression (Figure 5B), while the concomitant reduction of HSP72 and HSC70 (Supplemental Figure 11) was not observed, possibly because of posttranslational compensatory mechanisms (Qian *et al.*, 2006; Mao *et al.*, 2013). Inhibition of the HSP90 chaperone activity was further supported by depletion of its client proteins RAF1 and TrkA (Figure 5B).

In an attempt to perform a rescue experiment overexpressing HSP90, we realized that the extremely high level of HSP90 in these NB cells was making it impossible. As estimated from infection of CHP134 cells with lentiviral particles carrying either HSP90 cDNA or EGFP and luciferase reporters, the average expression level of ectopic HSP90 transcripts is not more than one thirtieth of the endogenous one, rendering it challenging to change the level of this protein exogenously (Supplemental Figure 12). To overcome this technical hindrance, we followed an alternative approach to investigate the impact of HSP90 targeting by CPX. We evaluated whether the combination of CPX treatment, affecting HSP90 translational efficiency and finally protein abundance, and of pharmacological inhibition of the HSP90 ATPase activity could synergize in terms of their effects on viability. Therefore, CHP134 cells were treated with CPX in combination with 17-allylamino,17-demethoxygeldanamycin (17AAG), a potent inhibitor of HSP90 activity. A synergism of the two molecules was observed for cell viability at the concentrations below EC50, as shown by the combination index (CI) versus fraction affected (Fa) plot (Figure

5C). Thus, CPX treatment sensitized CHP134 cells to pharmacological HSP90 inhibition, indicating the active role of CPX in HSP90 downregulation.

Overall, our data demonstrate the ability of CPX to translationally reduce HSP90 protein levels. Based on the iron-dependent mechanism of this inhibition, we hypothesized that this effect might be attributable to iron chelators in general. Therefore, we investigated if the other iron chelators would result in HSP90 downregulation. CHP134 cells were treated for 24 and 48 hours with piroctone, 8HQ and deferasirox, the three most potent and specific intracellular iron chelators resulted from our limited screen (Figure 1B, C). For each compound the effective concentrations for treatment were selected slightly below IG50 values based on the viability curves in Figure 1B and corresponded to 2 μM for piroctone, 3 μM for 8HQ, and 20 μM for deferasirox. As shown in Figure 5D, treatment of CHP134 cells with these iron chelators reduced the levels of both HSP90 and its client proteins. Thus, not only CPX but certain other iron chelators evoked a cellular response that downregulated HSP90 protein levels.

In summary, our preclinical results qualify CPX and few other iron chelators as candidates for further drug development and exploration in NB therapy. One potential drawback could result from the fact that the effect of iron chelators on cancer cells is multifactorial, and therefore could potentially interfere with conventional chemotherapeutics. In our cell model a combined treatment of CPX and topotecan or cisplatin, two chemotherapeutic drugs used for second-line treatment of NB, resulted in no antagonism for the first and slight synergism for the second (Supplemental Figure 13). The obvious advantage, instead, is that some iron chelators, including CPX, are already approved by the Food and Drugs Administration and thus do not need further preclinical trials to evaluate toxicity, thus providing a potential shortcut for drug reposition.

Molecular Pharmacology Fast Forward. Published on January 6, 2015 as DOI: 10.1124/mol.114.095729
This article has not been copyedited and formatted. The final version may differ from this version.

DISCUSSION

Iron is a crucial component of a variety of cellular pathways that are essential for cell replication, metabolism and growth (Richardson *et al.*, 2009; Torti and Torti, 2013). Iron enables the function of vital iron- and heme-containing enzymes including mitochondrial and detoxifying enzymes, enzymes involved in DNA synthesis, cell cycle, etc. Cancer cells have higher iron requirements possibly due to their rapid rate of proliferation. Hence, pathways of iron metabolism are often perturbed in cancer cells making them different to their non-malignant counterparts (Torti and Torti, 2013). Therefore, targeting iron-dependent pathways/proteins may selectively kill cancer cells with minimal damages for normal cells.

Iron chelators are agents that bind iron with a high affinity (Richardson *et al.*, 2009). They may act by withdrawing iron leading to tumor growth inhibition. Alternatively or additionally, they may form redox-active iron complexes resulting in the formation of reactive oxygen species, damaging critical intracellular targets and thereby eliciting a cytotoxic response. Iron chelators have demonstrated potent anti-neoplastic properties in a number of cancers *in vitro* and some of them, including CPX, DFO, deferasirox, are currently under preclinical or early clinical investigation as anticancer therapeutics (Torti and Torti, 2013). Among various tumors, the use of iron chelators as possible adjunct to NB therapy has been also investigated. In particular DFO, the first and most frequently studied chelator in NB, was reported to exert anti-proliferative effects on NB cells, with minimal effects on viability of non-cancerous cells and non-NB tumor cells (Blatt and Stitely, 1987; Becton and Bryles, 1988). With these promising preclinical results and owing to its safety profile, DFO anti-tumor activity was investigated in clinical trials. DFO was used in patients with NB either as monotherapy (Donfrancesco *et al.*, 1990) or as a part of

Molecular Pharmacology Fast Forward. Published on January 6, 2015 as DOI: 10.1124/mol.114.095729
This article has not been copyedited and formatted. The final version may differ from this version.

combination chemotherapy (Donfrancesco *et al.*, 1995), showing some promising preliminary results. In a different clinical study, however, DFO failed to produce partial or complete response in children with recurrent NB (Blatt, 1994). Moreover, DFO treatment was ineffective at inhibiting the growth of human NB xenografts (Selig *et al.*, 1998). This discrepancy in results could be due to a number of factors, including DFO intravenous route of administration combined to short plasma half-life, raising a need for long infusions to exert its effect (Kalinowski and Richardson, 2005). In addition, the highly hydrophilic nature of DFO severely limits its membrane permeability and hence the efficiency (Breuer *et al.*, 1995a). These limitations of DFO prompted an extended search for more effective iron chelators. Experiments with newer synthetic iron chelators, Triapine and 311, corroborated the data observed upon DFO treatment, namely the greater susceptibility to iron chelation of NB cells compared to normal cell types (Chaston *et al.*, 2003). In comparison with DFO, both Triapine and 311 demonstrated a greater anti-proliferative effect on the NB cells tested.

In this report we evaluated the potential of 17 compounds with reported iron chelation properties to inhibit the growth of NB in cell culture. Among the compounds tested, seven demonstrated concentration-dependent effect on viability of two NB cell lines with IG_{50} ranging over a 10-fold spectrum (from approximately 2 μM for piroctone to about 70 μM for deferiprone); five of seven compounds were shown to efficiently chelate intracellular iron. Among the iron chelators tested, CPX was of special interest because it has an acceptable toxicity profile and is currently evaluated as anticancer agent in a phase I study in patients with advanced hematologic malignancies (Weir *et al.*, 2011; Minden *et al.*, 2014). As indicated by our data, CPX exerted strong anti-proliferative activity on NB cells that could be reversed, at least partially, by loading the cells with iron, suggesting that the primary mechanism of CPX action is via iron sequestration. Of note, IG_{50} values of about

Molecular Pharmacology Fast Forward. Published on January 6, 2015 as DOI: 10.1124/mol.114.095729
This article has not been copyedited and formatted. The final version may differ from this version.

1-10 μM detected in CPX-treated NB cells are pharmacologically achievable (Weir *et al.*, 2011; Minden *et al.*, 2014). CPX-mediated effect on viability of NB cells resulted from a combination of cell cycle deregulation and induction of apoptosis, corroborating previously published data on other tumor cell types (Zhou *et al.*, 2010).

Interestingly, the effects of CPX on cell cycle distribution of CHP134 cells suggest that the CPX mode of action has a dose threshold in the concentration region between 2 and 6 μM. At the concentrations below the threshold CPX slows down cell cycle progression, while at the concentrations above the threshold CPX efficiently blocks the cells in the G_0/G_1 phase. This could be due to the capacity to target only a subset of iron-dependent proteins at lower concentrations, while for inhibiting other proteins higher concentrations of CPX could be needed. Several enzymes have been reported to be cellular targets for CPX, including ribonucleotide reductase (Eberhard *et al.*, 2009) and DOHH (Clement *et al.*, 2002; Mémin *et al.*, 2014). Ribonucleotide reductase is a rate-limiting enzyme in DNA synthesis responsible for converting nucleoside diphosphates to deoxynucleoside diphosphates. Therefore, the augmentation of NB cell number in the EdU+ population and contemporary decrease of its median fluorescence intensity might reflect an inhibition of the elongation step in DNA synthesis that could be attributable to the inhibition of ribonucleotide reductase. DOHH is the metalloenzyme catalyzing the final step in hypusine biosynthesis on the eIF5A translation factor. Hypusination of eIF5A is essential for its activity in promoting cell proliferation and survival (Park, 2006; Caraglia *et al.*, 2013). CPX has been reported to inhibit DOHH both in biochemical (Csonga *et al.*, 1996) and cellular assays (Clement *et al.*, 2002; Mémin *et al.*, 2014). Moreover, inhibition of DOHH was shown to coincide with proliferative arrest in the late G_1 phase of cell cycle (Hanauske-Abel *et al.*, 1994). Hence, G_0/G_1 arrest might result from CPX-mediated inhibition of DOHH. Interestingly, CPX exerted inhibition of DOHH in HUVEC and HeLa cells in a

Molecular Pharmacology Fast Forward. Published on January 6, 2015 as DOI: 10.1124/mol.114.095729
This article has not been copyedited and formatted. The final version may differ from this version.

concentration-dependent manner with the IC_{50} value of 5 and 6.25 μM, respectively (Clement *et al.*, 2002; Mémin *et al.*, 2014), coincident with the dose threshold region of CPX effects observed in CHP134 cells. In addition to DOHH, the G_1 arrest induced by CPX could be mediated by multiple mechanisms involving cyclin D1, CDK2, RB1, CDK inhibitor $p21^{CIP1/WAF1}$ (Zhou *et al.*, 2010). However, the link between these proteins and upstream iron-dependent events remains unclear.

We involved the HSP family as a potential CPX target through a two-level mRNA profiling study. HSPs are essential for cellular homeostasis by mediating correct protein folding, preventing protein aggregation, contributing to cell survival via inhibition of apoptosis, etc. Given the cytoprotective function of HSPs, it is not surprising that cancer cells often become addicted to HSPs, which is reflected by abnormal high expression and/or activity of some family members (Jego *et al.*, 2013). As a consequence, HSPs are emerging as promising targets in cancer therapy, particularly HSP90, which controls numerous oncogenic pathways (Trepel *et al.*, 2010). In fact, de Preter et al. (De Preter *et al.*, 2009) applying an integrative genomic meta-analysis approach on primary NB tumors and normal fetal neuroblasts predicted a putative therapeutic effect for a class of HSP90 inhibitors; a functional activity of the representative compound, 17-AAG, was subsequently confirmed in viability assays. Our data corroborate the reported findings showing that 17-AAG indeed significantly reduced viability of NB cells. Most importantly, we were able to demonstrate that CPX treatment sensitized neuroblastoma cells to 17-AAG-mediated inhibition of HSP90 activity.

One of the hallmarks of HSP90 inhibition, along with client proteins degradation, is the subsequent induction of HSP70 (Maloney *et al.*, 2007). This up-regulation hinders effective action of HSP90 inhibitors protecting the cells from it. Differently, upon treatment with CPX no induction of HSP70 proteins could be observed along with inhibition of HSP90,

Molecular Pharmacology Fast Forward. Published on January 6, 2015 as DOI: 10.1124/mol.114.095729
This article has not been copyedited and formatted. The final version may differ from this version.

pointing out the mechanism of CPX action different to conventional HSP90 inhibitors and rendering it particulary interesting for therapy. In line with this, a recent work of Mémin et al. (Mémin *et al.*, 2014) described that CPX resulted in hypusyl-eIF5A-mediated translational downregulation of yet another member of the HSP group, HSP27. Our data corroborate these findings, though at 24 hours we detect CPX-mediated inhibition of HSP27 both at the transcriptome and translatome levels (data not shown). It is appealing to assume that also HSP90 downregulation could be a consequence of deficient hypusyl-eIF5A. Moreover, HSP90 has been identified as a potential interaction partner of eIF5A and its modifying enzymes (Sievert *et al.*, 2012).

The activity on HSP90 of CPX is shared by the other three iron chelators demonstrated to induce a relevant cytotoxicity in NB cells. Of these, piroctone belongs to the same group of hydroxypirimidine derivatives of CPX, while 8HQ and deferasirox belong to different chemical classes. Therefore, the chemical property of iron chelation exerted intracellulary is the key determinant to reduction of translational efficiency of HSP90 and NB cell toxicity in this study.

In summary, we identify a potential mechanism by which CPX and other iron chelators act in NB cells to suppress viability – downregulation of HSP90 translation. Future detailed dissection of this and other key molecular targets of the active compounds we investigated could pave the way for efficient drug combination in the treatment of high-risk NB patients.

Molecular Pharmacology Fast Forward. Published on January 6, 2015 as DOI: 10.1124/mol.114.095729
This article has not been copyedited and formatted. The final version may differ from this version.

ACKNOWLEDGMENTS

We thank Erik Dassi for discussions on microarray data analysis and Emanuela Kerschbamer for technical assistance in the initial phase of the project. We are also grateful to Michael Pancher for sharing his expertise in the three-dimensional multicellular spheroids model.

Molecular Pharmacology Fast Forward. Published on January 6, 2015 as DOI: 10.1124/mol.114.095729
This article has not been copyedited and formatted. The final version may differ from this version.

AUTHORSHIP CONTRIBUTIONS

Participated in research design: Sidarovich, Adami, Tonini, Quattrone.

Conducted experiments: Sidarovich, Adami, Gatto, Greco.

Performed data analysis: Sidarovich, Gatto, Tebaldi.

Wrote or contributed to the writing of the manuscript: Sidarovich, Tebaldi, Quattrone.

Molecular Pharmacology Fast Forward. Published on January 6, 2015 as DOI: 10.1124/mol.114.095729
This article has not been copyedited and formatted. The final version may differ from this version.

REFERENCES

Arava Y, Wang Y, Storey JD, Liu CL, Brown PO, and Herschlag D (2003) Genome-wide analysis of mRNA translation profiles in Saccharomyces cerevisiae. *Proc Natl Acad Sci USA* **100**:3889–3894.

Becton DL, and Bryles P (1988) Deferoxamine inhibition of human neuroblastoma viability and proliferation. *Cancer Res* **48**:7189–7192.

Blatt J (1994) Deferoxamine in children with recurrent neuroblastoma. *Anticancer Res* **14**:2109–2112.

Blatt J, and Stitely S (1987) Antineuroblastoma activity of desferoxamine in human cell lines. *Cancer Res* **47**:1749–1750.

Blatt J, Taylor SR, and Kontoghiorghes GJ (1989) Comparison of activity of deferoxamine with that of oral iron chelators against human neuroblastoma cell lines. *Cancer Res* **49**:2925–2927.

Breuer W, Epsztejn S, and Cabantchik ZI (1995a) Iron acquired from transferrin by K562 cells is delivered into a cytoplasmic pool of chelatable iron(II). *J Biol Chem* **270**:24209–24215.

Breuer W, Epsztejn S, Millgram P, and Cabantchik IZ (1995b) Transport of iron and other transition metals into cells as revealed by a fluorescent probe. *Am J Physiol* **268**:C1354–C1361.

Brodeur GM (2003) Neuroblastoma: biological insights into a clinical enigma. *Nat Rev Cancer* **3**:203–216.

Burkhart CA, Cheng AJ, Madafiglio J, Kavallaris M, Mili M, Marshall GM, Weiss WA, Khachigian LM, Norris MD, and Haber M (2003) Effects of MYCN antisense oligonucleotide administration on tumorigenesis in a murine model of neuroblastoma. *J Natl Cancer Inst* **95**:1394–1403.

Caraglia M, Park MH, Wolff EC, Marra M, and Abbruzzese A (2013) eIF5A isoforms and cancer: two brothers for two functions? *Amino Acids* **44**:103–109.

Chaston TB, Lovejoy DB, Watts RN, and Richardson DR (2003) Examination of the antiproliferative activity of iron chelators: multiple cellular targets and the different mechanism of action of triapine compared with desferrioxamine and the potent pyridoxal isonicotinoyl hydrazone analogue 311. *Clin Cancer Res* **9**:402–414.

Cheung N-K V, and Dyer MA (2013) Neuroblastoma: developmental biology, cancer genomics and immunotherapy. *Nat Rev Cancer* **13**:397–411.

Clement PMJ, Hanauske-Abel HM, Wolff EC, Kleinman HK, and Park MH (2002) The antifungal drug ciclopirox inhibits deoxyhypusine and proline hydroxylation, endothelial cell growth and angiogenesis in vitro. *Int J Cancer* **100**:491–498.

Cole KA, and Maris JM (2012) New strategies in refractory and recurrent neuroblastoma: translational opportunities to impact patient outcome. *Clin Cancer Res* **18**:2423–2428.

Csonga R, Ettmayer P, Auer M, Eckerskorn C, Eder J, and Klier H (1996) Evaluation of the metal ion requirement of the human deoxyhypusine hydroxylase from HeLa cells using a novel enzyme assay. *FEBS Lett* **380**:209–214.

De Preter K, De Brouwer S, Van Maerken T, Pattyn F, Schramm A, Eggert A, Vandesompele J, and Speleman F (2009) Meta-mining of neuroblastoma and neuroblast gene expression profiles reveals candidate therapeutic compounds. *Clin Cancer Res* **15**:3690–3696.

Donfrancesco A, De Bernardi B, Carli M, Mancini A, Nigro M, De Sio L, Casale F, Bagnulo S, Helson L, and Deb G (1995) Deferoxamine followed by cyclophosphamide, etoposide, carboplatin, thiotepa, induction regimen in advanced neuroblastoma: preliminary results. Italian Neuroblastoma Cooperative Group. *Eur J Cancer* **31A**:612–615.

Donfrancesco A, Deb G, Dominici C, Pileggi D, Castello MA, and Helson L (1990) Effects of a single course of deferoxamine in neuroblastoma patients. *Cancer Res* **50**:4929–4930.

Eberhard Y, McDermott SP, Wang X, Gronda M, Venugopal A, Wood TE, Hurren R, Datti A, Batey RA, Wrana J, Antholine WE, Dick JE, Dick J, and Schimmer AD (2009) Chelation of intracellular iron with the antifungal agent ciclopirox olamine induces cell death in leukemia and myeloma cells. *Blood* **114**:3064–3073.

Hanauske-Abel HM, Park MH, Hanauske AR, Popowicz AM, Lalande M, and Folk JE (1994) Inhibition of the G1-S transition of the cell cycle by inhibitors of deoxyhypusine hydroxylation. *Biochim Biophys Acta* **1221**:115–124.

Hellemans J, Mortier G, De Paepe A, Speleman F, and Vandesompele J (2007) qBase relative quantification framework and software for management and automated analysis of real-time quantitative PCR data. *Genome Biol* **8**:R19.

Huang DW, Sherman BT, and Lempicki RA (2009) Systematic and integrative analysis of large gene lists using DAVID bioinformatics resources. *Nat Protoc* **4**:44–57.

Huang M, and Weiss WA (2013) Neuroblastoma and MYCN. *Cold Spring Harb Perspect Med* **3**: a014415.

Jego G, Hazoumé A, Seigneuric R, and Garrido C (2013) Targeting heat shock proteins in cancer. *Cancer Lett* **332**:275–285.

Kalinowski DS, and Richardson DR (2005) The evolution of iron chelators for the treatment of iron overload disease and cancer. *Pharmacol Rev* **57**:547–583.

Kontoghiorghes GJ, Piga A, and Hoffbrand AV (1986) Cytotoxic effects of the lipophilic iron chelator omadine. *FEBS Lett* **204**:208–212.

Ma TC, Langley B, Ko B, Wei N, Gazaryan IG, Zareen N, Yamashiro DJ, Willis DE, and Ratan RR (2012) A screen for inducers of p21(waf1/cip1) identifies HIF prolyl hydroxylase inhibitors as neuroprotective agents with antitumor properties. *Neurobiol Dis* **49**:13–21.

Maloney A, Clarke PA, Naaby-Hansen S, Stein R, Koopman J-O, Akpan A, Yang A, Zvelebil M, Cramer R, Stimson L, Aherne W, Banerji U, Judson I, Sharp S, Powers M, DeBilly E, Salmons J, Walton M, Burlingame A, Waterfield M, and Workman P (2007) Gene and protein expression profiling of human ovarian cancer cells treated with the heat shock protein 90 inhibitor 17-allylamino-17-demethoxygeldanamycin. *Cancer Res* **67**:3239–3253.

Mao R-F, Rubio V, Chen H, Bai L, Mansour OC, and Shi Z-Z (2013) OLA1 protects cells in heat shock by stabilizing HSP70. *Cell Death Dis* **4**:e491.

Mémin E, Hoque M, Jain MR, Heller DS, Li H, Cracchiolo B, Hanauske-Abel HM, Pe'ery T, and Mathews MB (2014) Blocking eIF5A modification in cervical cancer cells alters the expression of cancer-related genes and suppresses cell proliferation. *Cancer Res* **74**:552–562.

Minden MD, Hogge DE, Weir SJ, Kasper J, Webster DA, Patton L, Jitkova Y, Hurren R, Gronda M, Goard CA, Rajewski LG, Haslam JL, Heppert KE, Schorno K, Chang H, Brandwein JM, Gupta V, Schuh AC, Trudel S, Yee KWL, Reed GA, and Schimmer AD (2014) Oral ciclopirox olamine displays biological activity in a phase I study in patients with advanced hematologic malignancies. *Am J Hematol* **89**:363–368.

Park MH (2006) The post-translational synthesis of a polyamine-derived amino acid, hypusine, in the eukaryotic translation initiation factor 5A (eIF5A). *J Biochem* **139**:161–169.

Qian S-B, McDonough H, Boellmann F, Cyr DM, and Patterson C (2006) CHIP-mediated stress recovery by sequential ubiquitination of substrates and Hsp70. *Nature* **440**:551–555.

Richardson DR, Kalinowski DS, Lau S, Jansson PJ, and Lovejoy DB (2009) Cancer cell iron metabolism and the development of potent iron chelators as anti-tumour agents. *Biochim Biophys Acta* **1790**:702–717.

Schroeder T (2011) Long-term single-cell imaging of mammalian stem cells. *Nat Methods* **8**:S30–S35.

Schwanhäusser B, Busse D, Li N, Dittmar G, Schuchhardt J, Wolf J, Chen W, and Selbach M (2011) Global quantification of mammalian gene expression control. *Nature* **473**:337–342.

Selig RA, White L, Gramacho C, Sterling-Levis K, Fraser IW, and Naidoo D (1998) Failure of iron chelators to reduce tumor growth in human neuroblastoma xenografts. *Cancer Res* **58**:473–478.

Sen S, Hassane DC, Corbett C, Becker MW, Jordan CT, and Guzman ML (2013) Novel mTOR inhibitory activity of ciclopirox enhances parthenolide antileukemia activity. *Exp Hematol* **41**:799–807.

Sidarovich V, Adami V, and Quattrone A (2014) A Cell-Based High-Throughput Screen Addressing 3'UTR-Dependent Regulation of the MYCN Gene. *Mol Biotechnol* **56**:631–643.

Sievert H, Venz S, Platas-Barradas O, Dhople VM, Schaletzky M, Nagel C-H, Braig M, Preukschas M, Pällmann N, Bokemeyer C, Brümmendorf TH, Pörtner R, Walther R, Duncan KE, Hauber J, and Balabanov S (2012) Protein-protein-interaction network organization of the hypusine modification system. *Mol Cell Proteomics* **11**:1289–1305.

Song S, Christova T, Perusini S, Alizadeh S, Bao R-Y, Miller BW, Hurren R, Jitkova Y, Gronda M, Isaac M, Joseph B, Subramaniam R, Aman A, Chau A, Hogge DE, Weir SJ, Kasper J, Schimmer AD, Al-awar R, Wrana JL, and Attisano L (2011) Wnt inhibitor screen reveals iron dependence of β-catenin signaling in cancers. *Cancer Res* **71**:7628–7639.

Tebaldi T, Dassi E, Kostoska G, Viero G, and Quattrone A (2014) tRanslatome: an R/Bioconductor package to portray translational control. *Bioinformatics* **30**:289–291.

Tebaldi T, Re A, Viero G, Pegoretti I, Passerini A, Blanzieri E, and Quattrone A (2012) Widespread uncoupling between transcriptome and translatome variations after a stimulus in mammalian cells. *BMC Genomics* **13**:220.

Thiele CJ, Reynolds CP, and Israel MA (1985) Decreased expression of N-myc precedes retinoic acid-induced morphological differentiation of human neuroblastoma. *Nature* **313**:404–406.

Torti SV, and Torti FM (2013) Iron and cancer: more ore to be mined. *Nat Rev Cancer* **13**:342–355.

Trepel J, Mollapour M, Giaccone G, and Neckers L (2010) Targeting the dynamic HSP90 complex in cancer. *Nat Rev Cancer* **10**:537–549.

Weir SJ, Patton L, Castle K, Rajewski L, Kasper J, and Schimmer AD (2011) The repositioning of the anti-fungal agent ciclopirox olamine as a novel therapeutic agent for the treatment of haematologic malignancy. *J Clin Pharm Ther* **36**:128–134.

Zhou H, Shen T, Luo Y, Liu L, Chen W, Xu B, Han X, Pang J, Rivera CA, and Huang S (2010) The antitumor activity of the fungicide ciclopirox. *Int J Cancer* **127**:2467–2477.

Molecular Pharmacology Fast Forward. Published on January 6, 2015 as DOI: 10.1124/mol.114.095729
This article has not been copyedited and formatted. The final version may differ from this version.

FOOTNOTES

This work was supported by a grant from the Italian Neuroblastoma Foundation.

Molecular Pharmacology Fast Forward. Published on January 6, 2015 as DOI: 10.1124/mol.114.095729
This article has not been copyedited and formatted. The final version may differ from this version.

Figure 1. Identification of iron chelators with antiproliferative activity in NB cells.

(A) CHP134 cells were treated for 48 hours with 1 μM and 10 μM of CPX (1), DFO (2), deferasirox (3), piroctone olamine (4), 8HQ (5), deferiprone (6), D-(–)- tagatose (7), 2,2'-bipyridyl (8), omadine (9), 2,3-dihydroxybenzoic acid (10), DTPA (11), o-phenantroline (12), 2-picolinic acid (13), L-mimosine (14), ferrichrome (15), dexrazoxane (16), ferrozine (17). Cell viability was measured by AlamarBlue assay. The data represent the mean ± SD of three measurements. (B) CHP134 and SiMa cells were treated with 0.33-100 μM of CPX, DFO, deferasirox, piroctone olamine, 8HQ, deferiprone, and omadine for 48 hours. Cell viability was measured by AlamarBlue assay. Data represent the mean percentage of viable cells ± SD from three measurements. (C) SiMa cells were loaded with the intracellular iron-chelating fluorescent dye calcein-AM. Cells were treated with the compounds indicated in (B) for 10 minutes (all at 10 μM, but DFO at 100 μM). Intracellular iron bound by calcein was measured by flow cytometry. Percentage increase ± SD in the median intracellular calcein fluorescence of three replicates is shown.

Figure 2. CPX reduces viability of NB cells in an iron dependent manner.

MNA (A) and non-MNA (B) NB cells as well as non-NB (C) cells were treated with increasing concentrations of CPX with (shown only for CHP134) or without iron in form of HT. 48 hours after cell viability was measured by AlamarBlue assay. Data represent the mean percentage of viable cells ± SD from one of at least three representative experiments. (D) Growth curves of CHP134 cells treated with CPX with (shown only for 20 μM concentration) and without iron. Cellular growth was monitored on the xCELLigence System (Roche). Raw read-outs were normalized against the value read immediately after compounds addition (first dashed vertical line). Each curve represents the mean ± SEM at every single time point. (E) CHP134 cells growing as 3D multicellular spheroids were

Molecular Pharmacology Fast Forward. Published on January 6, 2015 as DOI: 10.1124/mol.114.095729
This article has not been copyedited and formatted. The final version may differ from this version.

treated with CPX (0-20 μM) with or without iron in form of HT. Spheroids were imaged after 48, 72 and 96 hours of treatment using a high-content imaging system Operetta (PerkinElmer). The experiment was performed three times in technical quadruplicate. The representative images of spheroids are displayed.

Figure 3. CPX induces cell cycle arrest and apoptosis in CHP134 cells.

(A-C) Dose-dependent effects of CPX (0-20 μM, 24 hours) on cell cycle phase distribution. The cells were processed for cell cycle analysis using Click-iT EdU flow cytometry assay kit. (A) Representative Alexa-Fluor 488 EdU (exponential axis) and DNA 7-AAD histograms (linear axis) are displayed. (B) Dose response curve demonstrates the percentage of cells in G_0/G_1, S, and G_2/M phases from the data displayed in panel A. (C) Dose response curve showing the median fluorescence intensity of the EdU+ population from the data displayed in panel A. (D) CHP134 cells growing in 96-well plates were treated with CPX (0-20 μM) for 24 and 48 hours. A high-content imaging apoptosis assay was performed on fixed cells immunofluorescently labeled for activated caspase-3.

Figure 4. Genome-wide gene expression analysis reveals uncoupling of transcriptional and translational variations after CPX treatment, with a decrease in the translational efficiency of HSP genes.

(A) Pie chart highlighting the number and the percentage of differentially expressed genes (DEGs) falling in each uncoupling class. Genes are colored according to how they react to the treatment: cyan and blue for DEGs with significant variations only in the transcriptome, yellow and orange for DEGs with significant variations only in the translatome, red for DEGs with opposite significant variations, and green for DEGs with significant

homodirectional changes. Genes are further divided in either up-regulated or down-regulated. (B) Heatmap showing enrichment analysis of protein domains with the annotation provided by PFAM and INTERPRO. Enrichment False Discovery Rate (FDR) values are displayed, with significant values (<0.05) colored in blue shades. (C) Box whisker plot of log2 translational efficiency changes induced by CPX. Translational efficiencies are calculated as the ratio of translatome and transcriptome signals. The distribution of the whole set of human genes with microarray probes (in dark grey) is compared with the distribution of HSP protein families: HSP70, HSP40, HSP90 and the union of all HSP members.

Figure 5. CPX and other iron chelators downregulate HSP90 expression in CHP134 cells.

(A) qPCR of the HSP genes in the total and polysomal RNA fraction of CHP134 cells exposed to 5 μM CPX ± HT or HT alone for 24 hours. Relative expression levels were normalized using the geometric mean of *TBP*, *HPRT* and *SDHA* reference genes. The level of expression is shown relative to controls. Mean values ± SD are provided, n=3–5. Asterisks indicate statistical significance in two-tailed t-test, * P<0.05, ** P<0.01, *** P<0.001. (B) Immunoblots showing expression of HSP90 and its client proteins RAF1 and TrkA following treatment with 5 μM CPX for up to 48 hours. GAPDH was included as a loading control. (C) CHP134 cells growing in 96-well plates were treated with increasing concentrations of CPX and 17-AAG and their respective combination at constant ratio as indicated. Left panel displays cell viability measured in 48 hours by the AlamarBlue assay. Right panel represents data analyzed with the CompuSyn software, in which the combination index (CI) indicates synergism (CI<0.9), additivity (CI=0.9-1.1), or

Molecular Pharmacology Fast Forward. Published on January 6, 2015 as DOI: 10.1124/mol.114.095729
This article has not been copyedited and formatted. The final version may differ from this version.

antagonism (CI>1.1). The points correspond to experimental values and the curve is a trend line. All data represent the mean over three independent experiments. (D) Immunoblots showing expression of HSP90 and its client proteins RAF1 and TrkA following treatment with 2 μM piroctone, 3 μM 8HQ, and 20 μM deferasirox for up to 48 hours. GAPDH served as the loading control.

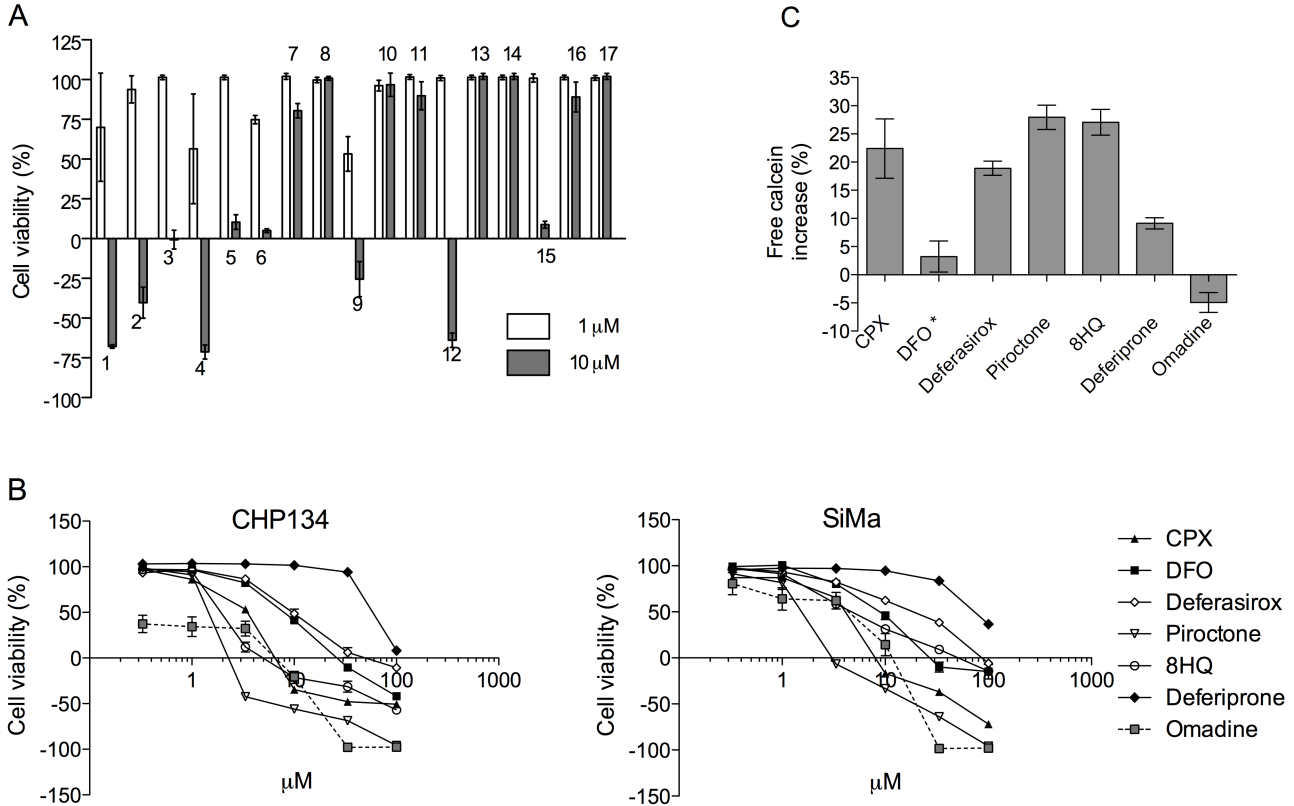
A
Cell viability (%)
125
100
75
50
25
0
-25
-50
-75
-100
1
2
3
4
5
6
7
8
9
10
11
12
13
14
15
16
17
1 μM
10 μM
C
Free calcein increase (%)
35
30
25
20
15
10
5
0
-5
-10
CPX
DFO *
Deferasirox
Piroctone
8HQ
Deferiprone
Omadine
B
CHP134
SiMa
Cell viability (%)
150
100
50
0
-50
-100
-150
1
10
100
1000
μM
CPX
DFO
Deferasirox
Piroctone
8HQ
Deferiprone
Omadine

Figure 1

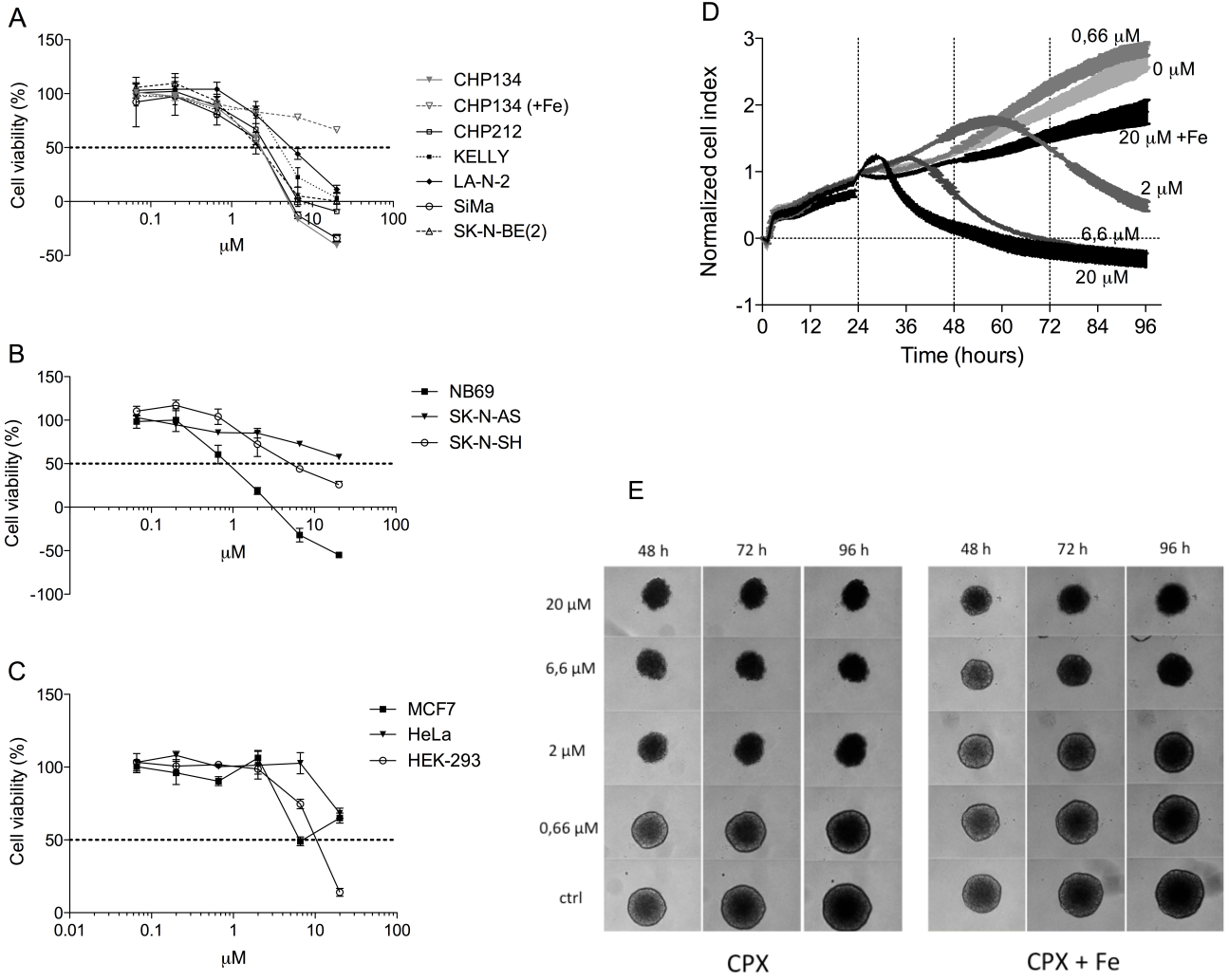
A
Cell viability (%)
150
100
50
0
-50
0.1
1
10
100
µM
CHP134
CHP134 (+Fe)
CHP212
KELLY
LA-N-2
SiMa
SK-N-BE(2)
B
Cell viability (%)
150
100
50
0
-50
-100
0.1
1
10
100
µM
NB69
SK-N-AS
SK-N-SH
C
Cell viability (%)
150
100
50
0
0.01
0.1
1
10
100
µM
MCF7
HeLa
HEK-293
D
Normalized cell index
3
2
1
0
-1
0
12
24
36
48
60
72
84
96
Time (hours)
0,66 µM
0 µM
20 µM +Fe
2 µM
6,6 µM
20 µM
E
48 h
72 h
96 h
48 h
72 h
96 h
20 µM
6,6 µM
2 µM
0,66 µM
ctrl
CPX
CPX + Fe

Figure 2

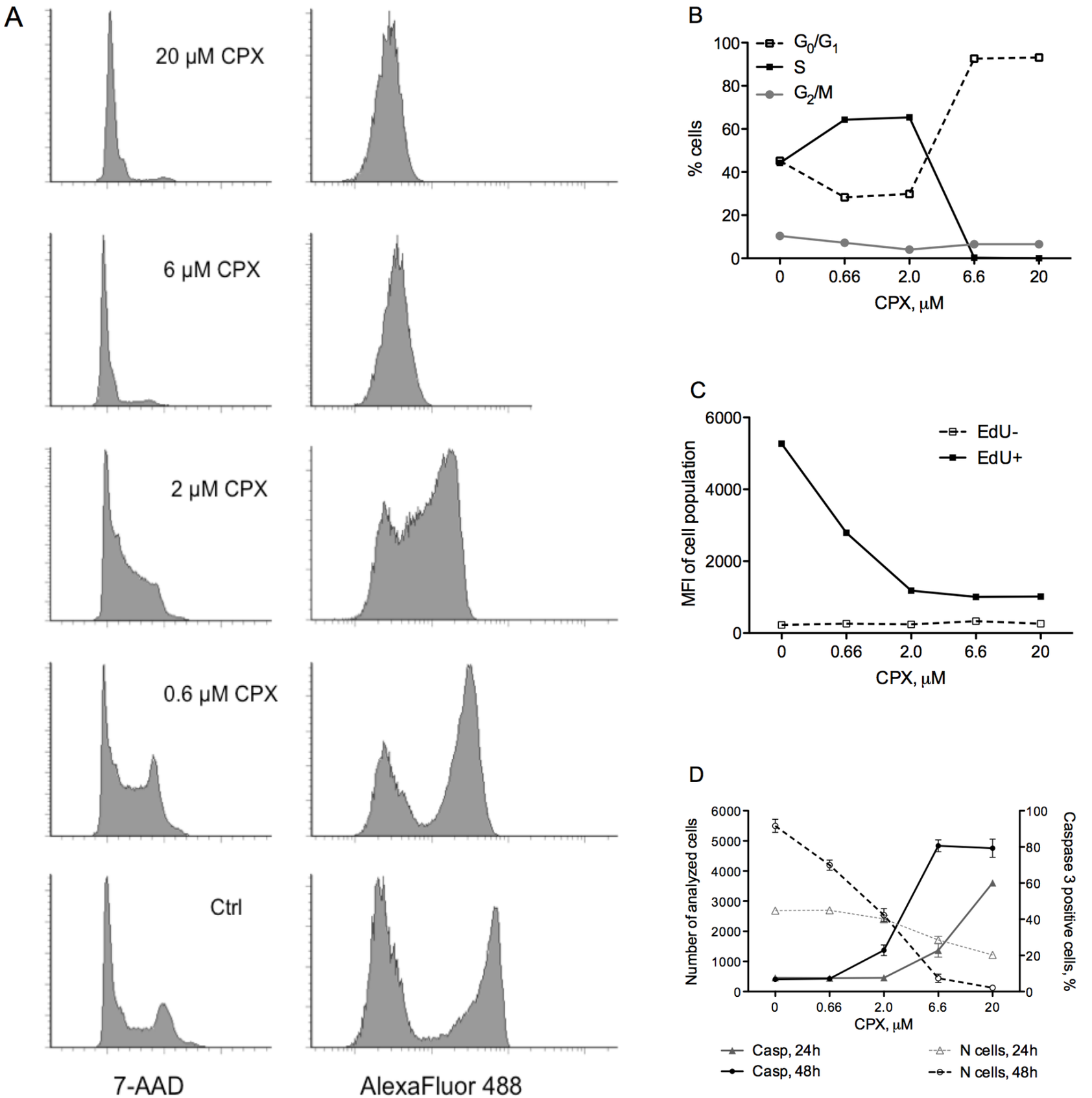
A
20 μM CPX
6 μM CPX
2 μM CPX
0.6 μM CPX
Ctrl
7-AAD
AlexaFluor 488
B
G0/G1
S
G2/M
% cells
CPX, μM
C
EdU-
EdU+
MFI of cell population
CPX, μM
D
Number of analyzed cells
Caspase 3 positive cells, %
CPX, μM
Casp, 24h
Casp, 48h
N cells, 24h
N cells, 48h

Figure 3

A

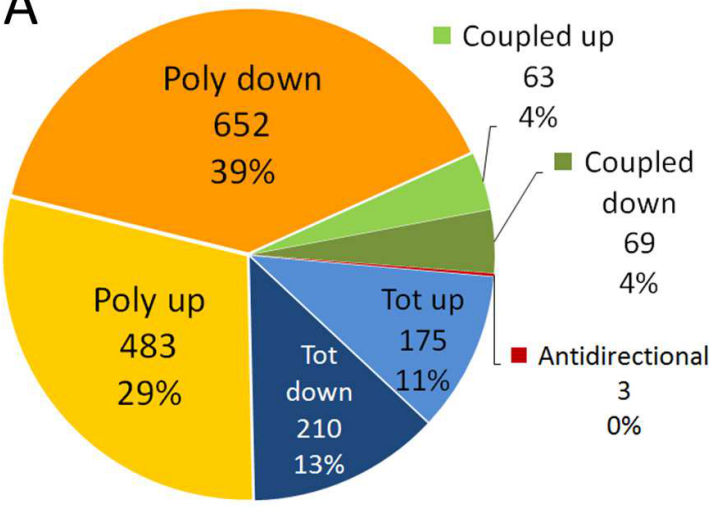

B

Source	Term	tot up	tot down	poly up	poly down
PFAM	Hsp70 protein	1.00E+00	1.00E+00	1.00E+00	2.06E-02
IPR	Heat shock protein 70	1.00E+00	1.00E+00	1.00E+00	2.27E-02
IPR	RNA recognition motif	1.00E+00	1.00E+00	1.00E+00	2.37E-02
IPR	WD40 repeat	1.00E+00	1.00E+00	1.00E+00	2.73E-02
IPR	Zinc finger, C2H2-type	7.34E-01	1.19E-18	1.07E-01	1.00E+00
PFAM	zf-C2H2	9.18E-01	2.96E-18	3.81E-01	1.00E+00
IPR	Krueppel-ass. box	1.00E+00	4.46E-13	1.00E+00	1.00E+00
PFAM	KRAB	1.00E+00	1.17E-12	1.00E+00	1.00E+00

C

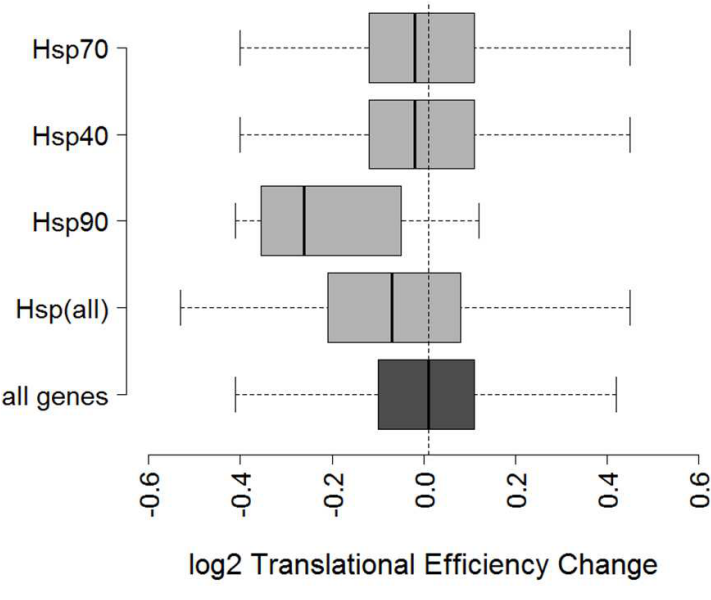

Figure 4

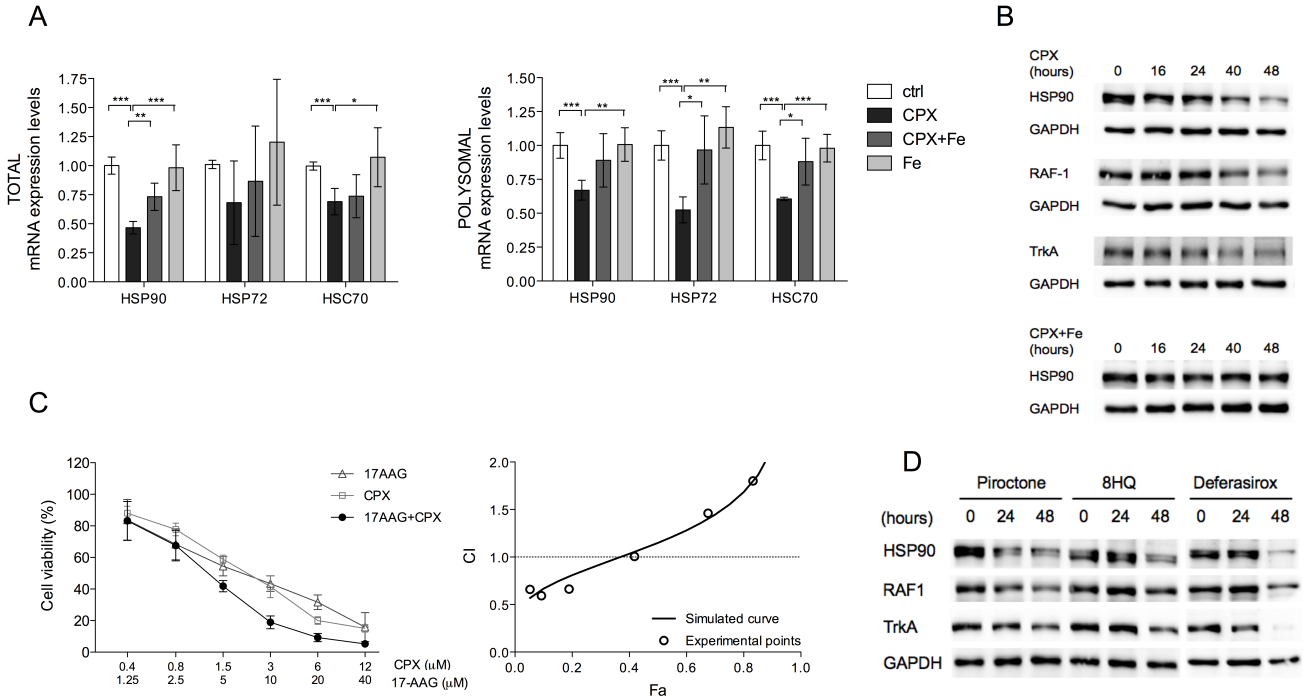
A
TOTAL
mRNA expression levels
1.75
1.50
1.25
1.00
0.75
0.50
0.25
0.00
HSP90
HSP72
HSC70
POLYSOMAL
mRNA expression levels
1.50
1.25
1.00
0.75
0.50
0.25
0.00
HSP90
HSP72
HSC70
ctrl
CPX
CPX+Fe
Fe
B
CPX
(hours)
0
16
24
40
48
HSP90
GAPDH
RAF-1
GAPDH
TrkA
GAPDH
CPX+Fe
(hours)
0
16
24
40
48
HSP90
GAPDH
C
Cell viability (%)
120
100
80
60
40
20
0
17AAG
CPX
17AAG+CPX
0.4
1.25
0.8
2.5
1.5
5
3
10
6
20
12
40
CPX (μM)
17-AAG (μM)
CI
2.0
1.5
1.0
0.5
0.0
0.0
0.2
0.4
0.6
0.8
1.0
Fa
Simulated curve
Experimental points
D
Piroctone
8HQ
Deferasirox
(hours)
0
24
48
0
24
48
0
24
48
HSP90
RAF1
TrkA
GAPDH

Figure 5